PCCP

Accepted Manuscript

This is an *Accepted Manuscript*, which has been through the Royal Society of Chemistry peer review process and has been accepted for publication.

Accepted Manuscripts are published online shortly after acceptance, before technical editing, formatting and proof reading. Using this free service, authors can make their results available to the community, in citable form, before we publish the edited article. We will replace this *Accepted Manuscript* with the edited and formatted *Advance Article* as soon as it is available.

You can find more information about *Accepted Manuscripts* in the Information for Authors.

Please note that technical editing may introduce minor changes to the text and/or graphics, which may alter content. The journal's standard Terms & Conditions and the Ethical guidelines still apply. In no event shall the Royal Society of Chemistry be held responsible for any errors or omissions in this *Accepted Manuscript* or any consequences arising from the use of any information it contains.

ROYAL SOCIETY OF CHEMISTRY

www.rsc.org/pccp

Journal Name

Cite this: DOI: 10.1039/c0xx00000x

www.rsc.org/xxxxxx

ARTICLE TYPE

Au@Ag Core-Shell Nanocubes: Epitaxial Growth Synthesis and Surface-Enhanced Raman Scattering Performance

Yanting Liu,[a] Jun Zhou,*[a] Binbing Wang,[a] Tao Jiang,[a] Ho-Pui Ho,[b] Lucia Petti[c] and Pasquale Mormile[c]

Received (in XXX, XXX) Xth XXXXXXXXX 201X, Accepted Xth XXXXXXXXX 201X

DOI: 10.1039/c0xx00000x

Novel Au@Ag core-shell nanocubes (NCs) were successfully prepared by the controlled epitaxial growth of Ag shells onto Au nanoellipsoids (NEs) in the presence of surfactants. The growth mechanism of the Au@Ag core-shell NCs was systematically investigated by analyzing their morphology, optical properties, and crystallography. The localized surface plasmon resonance (LSPR) characteristics and the electric field distribution of the Au@Ag core-shell NCs were studied using the finite element method (FEM) based on the plasmon hybridization theory. Compared with pure Ag NCs, the absorption spectrum of the Au@Ag core-shell NCs exhibits a red shift and a weak shoulder near 550 nm, and the notable enhancement of electric field occurs around the corners along the long-axis of Au ellipsoidal core because of plasmonic resonant coupling. Surface-enhanced Raman scattering (SERS) of the Au@Ag core-shell NCs labeled with 4-mercaptobenzoic acid molecules reveals that the bimetallic core-shell NCs possess efficient SERS activity with an enhancement factor EF = 2.27×10^6, thus confirming the possibility of using the Au@Ag core-shell NCs as stable probe for SERS-based biosensing applications.

1. Introduction

Noble metals nanomaterials have attracted considerable research efforts into their synthesis, characterization, and applications over several decades.[1-3]Among the nanomaterials reported, Au and Ag nanoparticles (NPs) are most popular and their geometry-dependent optical properties have been studied extensively. [4-6] In particular, the Au NPs has been very attractive because of their good biocompatibility, strong chemical resistance and ease in surface modification.[7] On the other hand, Ag NPs are well known to exhibit superior plasmonic response, strong electromagnetic enhancement, high sensitivity towards physical and chemical changes in their surrounding environment and low material cost.[8] These characteristics render them the materials of choice for possible applications in biological sensing,[9] medicine imaging,[10] drug delivery [11] and plasmon-driven catalysis reaction.[12]

Most recently, many effective strategies have been proposed to form bimetallic NPs owing to their novel multifunctional features such as optical, electronic, magnetic, and catalytic properties, which are different from individual metal nanostructures.[9] That is, the bimetallic nanostructures will combine the properties of the component materials or give rise to novel collective behaviors.[13] Naturally, the idea is motivated by controlling the morphology and size of individual metal NPs to systematically tailor the optical and plasmonic properties of these bimetallic NPs. As a typical sample of the binary metal nanostructures, the controllable synthesis of bimetallic core-shell NPs have been generously researched and intensely focused on varying their morphology to tune the optical properties in the visible range.[14]

Many methods have been explored for the synthesis of bimetallic core-shell NPs with controllable morphology. For instance, Han et al reported the synthesis of a new type of hybrid Pt/Au nanowires via galvanic replacement reaction between Pt nanowires and $AuCl_3$;[15] Lu et al proposed the generation of bimetallic Au-Pt nanorods by means of seed-mediated growth *in situ* in thermo-sensitive core-shell microgels;[16] Ayon et al synthesized Au/Ag bimetallic multi-spiked NPs by using a co-reduction reaction method.[17] On the other hand, the epitaxial growth method is a typical approach to prepare bimetallic core-shell nanocrystals through overgrowth of a different material on well-faceted seeds.[13, 18-19] Given that Au and Ag have the same face centered cubic (fcc) crystal structure with a very small lattice mismatch (lattice constants: Au 4.078 Å, Ag 4.086 Å), they can form various anisotropic bimetallic nanocrystal structures by the epitaxial growth method,[20] such as nanorod, stars, and polyhedron.[21-24] In particular, Au@Ag core-shell nanocubes (NCs) also have been successfully synthesized by using spherical or polyhedral Au seeds as core.[25, 26] In fact, the Au@Ag core-shell NCs are formed by integrating an Au core and an Ag shell into a cubic architecture with precise control on the geometry. Subsequently, the localized surface plasmon resonance (LSPR) of the Au@Ag core-shell NCs exhibits distinct geometry-dependence, which leads to a new way to tune the plasmon resonance wavelength for stronger surface electric field enhancement.[14, 27] The resultant surface-enhanced Raman scattering (SERS) from the Au@Ag core-shell NCs may offer better detection sensitivity of target molecules, [28, 29] which are directly relevant to sensing and imaging applications.[30, 31]

Physical Chemistry Chemical Physics Accepted Manuscript

Here, we report the synthesis of bimetallic Au@Ag core-shell NCs, which consist of Au nanoellipsoid core and Ag shell, through the epitaxial growth technique with the presence of surfactants. As mentioned above, plasmonic resonance coupling of Au core and Ag shell in Au@Ag core-shell NCs is the cause of the local surface electric field enhancement in the nanostructure, which may in turn lead to favourable performance in relation to SERS.

By analysing the spectroscopic and crystallographic characteristics, the growth mechanism of the Au@Ag core-shell NCs has been studied in detail which revealed that the growth was driven by a geometry-controlled colloidal synthesis process. To further understand the relationship between LSPR and the structure of the Au@Ag core-shell NCs such as the spacing between the ellipsoidal core and shell, the optical absorption spectra and the electric field intensity distributions of two types of nanocubic models were simulated using the finite element method (FEM). The simulation results are consistent with those obtained from experiments, and the physical origin of the LSPR and the enhanced electric field of Au@Ag core-shell NCs also have been reasonably explained based on the plasmonic hybridization theory. In addition, the SERS properties of the Au@Ag core-shell NCs were investigated with 4-mercaptobenzoic acid (4-MBA) as the Raman reporter molecule and a high SERS enhancement was demonstrated.

2. Materials and Methods

2.1 Materials

Hydrogen tetrachloroaurate (Ⅲ) trihydrate ($HAuCl_4$•$3H_2O$) and silver nitrate ($AgNO_3$) were purchased from Sigma Aldrich. Potassium bromide (KBr), cetyltrimethylammonium bromide (CTAB), cetyltrimethylammonium chlorine (CTAC) and cetylpyridinium chloride (CPC) were purchased from Aladdin. L-ascorbic acid (AA) was purchased from Bodi Chemical Reagents Co. (Tianjin, China). Sodium borohydride ($NaBH_4$) was purchased from Sinopharm Chemical Reagent Co. 4-Mercaptobenzoic acid (4-MBA) was obtained from J&K Chemical. Milli-Q water (18.2 MΩ•cm resistivity) was used for all solution preparations. All chemicals were in analytical grade and used as-received. Glasswares were cleaned by aqua regia and rinsed with deionized water several times prior to the experiments.

2.2 Synthesis of Au@Ag core-shell NCs

2.2.1 Synthesis of Au nanorods (NRs).

Au NRs were synthesized by a seed-mediated growth method.[32] Firstly, freshly-prepared ice cold $NaBH_4$ (600 μL, 10 mM) solution was added to the mixture of $HAuCl_4$ (250 μL, 10 mM) and CTAB (7.5 mL, 100mM) at 30°C, followed by vigorously stirring for 2 min. The seed solution with brownish color was formed. Secondly, the growth solution was prepared by mixing CTAB (4.75 mL, 100 mM), $HAuCl_4$ (200 μL, 10 mM), and $AgNO_3$ (30 μL, 10 mM). Then the growth solution immediately changed to colorless after the AA (32 μL, 100 mM) was added at 30°C. Finally, 10 μL of the seed solution was added to the growth solution with gently agitating for 20 s. The as-prepared solution gradually changed into pinkish-red color and undisturbedly aged at 30°C overnight. Afterwards, the as-synthesized Au NRs solution was centrifuged (11000 rpm, 30 min), and then re-dispersed in deionized water for further use.

2.2.2 Synthesis of Au nanoellipsoids (NEs)

A modified strategy was used to synthesis Au NEs.[33] The first step was a process of the secondary overgrowth of Au NRs. A 5 mL aliquot of the as-synthesized and purified Au NRs solution was centrifuged (11000 rpm, 20 min) again and dispersed in CTAB (5 mL, 10 mM) solution. Subsequently, $HAuCl_4$ solution (500μL, 10 mM) and AA (100μL, 100 mM) solution were added in order and mixed exhaustively. The mixture was permit to react at 40 °C for 1h. After that, the as-overgrown Au NRs solution were separated by centrifugation (11000 rpm, 30 min) and then re-dispersed in deionized water.

In the final step, Au NEs were prepared by using CPC as surfactant to convert the overgrown Au NRs to ellipsoidal nanoparticles.[33] Briefly, 5 mL of the as-overgrown Au NRs solution went through three washing cycles by centrifugation (11000 rpm, 20 min) to replace the CTAB-rich solution with CPC(5 mL, 100 mM) solution. Next, $HAuCl_4$ solution (100 μL, 10 mM) was added to the centrifuged solution and gently stirring for 30 s. After that, the mixed solution was left undisturbed and aged at 40 °C for 12 h. Finally, the as-synthesized Au NEs solutions were centrifuged (1000 rpm, 30 min) and re-dispersed in deionized water.

2.2.3 Epitaxial growth of Au@Ag core-shell NCs

The synthesis procedure of Au@Ag core-shell NCs is described as follows. Typically, 5 mL of the as-synthesized Au NEs solution was washed with 20 mM CTAC solution by three cycles centrifugation (20 min, 11000 rpm). The centrifuged solution was dispersed in ultrapure water as the seed solution to prepare the Au@Ag core-shell NCs. Thereafter, 100 μL of seed solution and KBr (100 μL, 10 mM) was added to CTAC (5 mL, 20 mM) solution with mixing. Successively, the mixture was heated at 60 °C for 10 min, then quickly added $AgNO_3$ (100μL, 10 mM) and AA (300 μL, 100 mM) all in once with pipette, and left undisturbed at 60 °C for 6 h to ensure the fully reduction of silver. Finally, the as-prepared Au@Ag core-shell NCs solution was centrifuged (11000 rpm, 30 min) and re-dispersed in deionized water for later characterization.

2.3 Instrumentation

UV-Vis absorption spectra were measured with spectrometer (TU1901, Pgeneral). SU-70 FESEM instrument was used to record the scanning electron microscopy (SEM) images under an accelerating voltage of 5 kV Transmission electron microscope (TEM), high-resolution transmission electron microscope (HRTEM) images, selective area electron diffraction (SAED) pattern and energy-dispersive X-ray analysis (EDAX) were obtained with TEM (JEM-2100F, JEOL) operated at accelerating voltage of 200 kV. All the analyses were performed at room temperature.

2.4 Calculation

A series of numerical calculations were carried out by using the incorporated RF module of the commercial software package (COMSOL Multiphysics 4.3). The electromagnetic properties of complex nanostructures can be readily handled by the finite element method (FEM) in an appropriate discrete spatial grid. In

Physical Chemistry Chemical Physics Accepted Manuscript

This journal is © The Royal Society of Chemistry [year]

our calculations, the frequency dependent dielectric functions for gold and silver are obtained from the bulk experimental result of Johnson and Christy.[34] The medium environment is presumed to be water with the refraction index of 1.33. According to the dimensions extracted from the TEM and SEM images in our experiments, a corner-truncated cubic model with an ellipsoidal Au core and Ag shell was constructed to simulate the optical absorption spectra and the electric field distributions in real Au@Ag core-shell NCs.

2.5 SERS Studies

To evaluate the SERS performance of the as-synthesized Au@Ag core-shell NCs, the sample solutions were prepared by adding an aliquot of 4-MBA (1 mM, 20 µL) solution to the above purified 5mL of Au@Ag core-shell NCs solutions under stirring and the resultant solutions were agitated for 5 h. Afterwards, the mixtures were centrifuged (11000 rpm, 20 min) for removing unbound 4-MBA molecules, and the 4-MBA-labeled Au@Ag core-shell NCs deposited to the bottom of reactive tubes. Next, the 4-MBA-labeled nanocubes were dispersed in 5 mL deionised water. Lastly, 1mL of the 4-MBA-labeled nanocube solutions was transfer to a 2 mm quartz cuvette. The SERS properties of the 4-MBA-labeled Au@Ag core-shell NCs were examined by the miniature Raman spectrometer (BWS415, B&W Tek Inc.) with a 785-nm semiconductor laser as the excitation source. Raman spectrographs were recorded with a laser power at the sample position of 49.55 mW and an accumulation time of 10 s. The scattered radiation was collected by a 20×objective lens with numerical aperture (NA) 0.4 and the wavelength dispersion was performed using a 1200 lines/mm grating, and then passed through a slit with 20 µm width to the charge-coupled device (CCD) (2048×2048 pixels) detector.

3. Results and discussion

3.1 Characterization of the Au NRs and Au NEs

Typical SEM images of the as-prepared Au NRs and overgrown Au NRs are shown in Fig. 1(a) and 1(b). It is seen that an average aspect ratio and an average length of the Au NRs are about 3.2 and 48 ± 3 nm, respectively; and the average aspect ratio and average length of the overgrown Au NRs are about 2.8 and 52 ± 2 nm, respectively. The SEM image of the as-prepared Au NEs is shown in Fig. 1(c), which reveals the overall ellipsoidal morphology with an average oblateness 0.42 and an average size 63 ± 5 nm. The evolution of the growth process from Au NRs to Au NEs has been studied by the UV-vis spectroscopy. And the absorption spectra of the Au NRs, the overgrown Au NRs and the Au NEs are shown in Fig. 1(d). From the black curve in Fig. 1(d), the spectrum of the Au NRs possess two principal plasmon absorption bands, a weak transverse plasmon resonance (TPR) band at 541 nm and a strong longitudinal plasmon resonance (LPR) band at 742 nm.[35] After an overgrown process, the Au NRs have become fatter, and consequently the LPR band of the overgrown Au NRs exhibits blue shifts (the blue curve). Finally, following the procedure of converting the overgrown Au NRs to ellipsoid nanoparticles, only one peak at 528 nm remains (the red curve), which confirms the formation of Au NEs.[33]

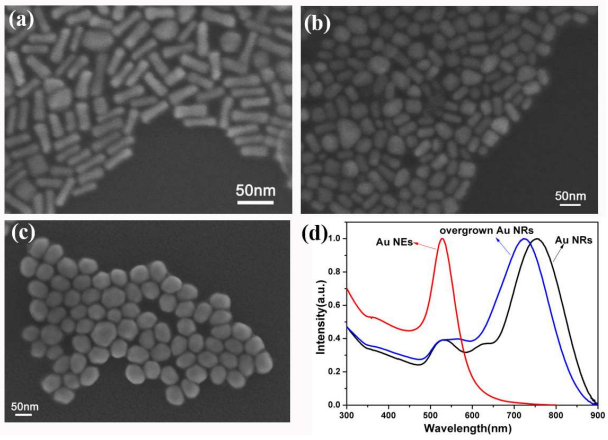

Fig. 1 SEM of (a) Au NRs, (b) overgrown Au NRs and (c) Au NEs, and (d) UV-vis absorption spectra of Au NRs (black curve), overgrown Au NRs (blue curve), and Au NEs (red curve).

3.2. Characterization of Au@Ag core-shell NCs

Au@Ag core-shell NCs were fabricated by using the as-synthesized Au NEs as cores for depositing Ag shell in an aqueous surfactant solution. Figure 2(a) shows the SEM image of the core-shell particles which exhibit uniform cubic shape with a mean size of 55 ± 5 nm. Size distributions and occupancy of Au@Ag core-shell NCs are provide in Fig. S1. The TEM image of the individual 57 nm Au@Ag core-shell NC is shown in Fig. 2(b) and indicates that the cube contains an Au ellipsoidal core at the center and a uniform single-crystalline Ag shell, in which the enhanced color contrast comes from the different atomic numbers between Au and Ag elements. Due to coating Ag shell on Au core, the absorption spectrum of Au@Ag core-shell NCs (Fig. 2(c)) exhibits three distinct plasmon peaks at 465, 351 and 394 nm, respectively, which is very resemble to that of pure Ag NCs with similar size (Fig. S2 and Fig. S3) and correspond to the LSPR coupling effects of dipole and multipole modes induced by the corners and edges of the nanocube. [36] However, there is a slight shoulder around 550 nm in Fig. 2(c), which may arise from the effect of plasmon mode of Au ellipsoidal core (see Fig. S3 (a) and Fig. S5, detailed analyses in the supporting information). Moreover, to further confirm the structure and composition of Au@Ag core-shell NCs, EDX analysis was carried out on a vast number of Au@Ag core-shell NCs. Fig. 2(d) indicates that there are two constituent elements Au and Ag in the nanocubes. From the above analysis, a complete conversion from the ellipsoid Au cores into the well-shaped core-shell NCs has been presented.

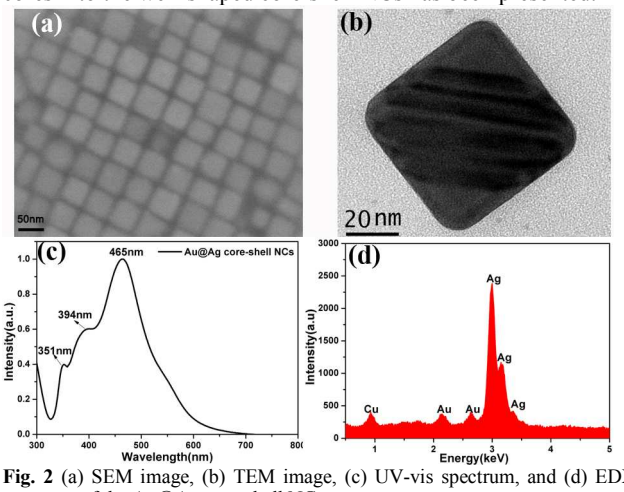

Fig. 2 (a) SEM image, (b) TEM image, (c) UV-vis spectrum, and (d) EDX spectrum of the Au@Ag core-shell NCs.

Physical Chemistry Chemical Physics Accepted Manuscript

On the other hand, the crystallographic characteristics of the Au@Ag core-shell NCs are also investigated to confirm the formation of heterogeneous single-crystal nanocubes. Fig. 3(a) and 3(b) give the HRTEM images of a single nanocrystal cube and the corresponding partial enlarged image, respectively. From Fig. 3(a), it clearly displays that the Au@Ag core-shell NC is a single nanocrystal cube bounded by {100} bare surface and do not contain defects at the boundary between Au core and Ag shell. According to the JCPDS no.87-0720, Fig. 3(a) also reveals a lattice spacing of 2.0 Å, indexing to {200} planes of face centered cubic (fcc) silver. In Fig. 3(b), the sharp corner of cube has been truncated, which results in its eight {111} facets being exposed to the surface of Ag shell. Fig. 3(c) is the SAED patterns corresponding to the Au@Ag core-shell NC. It further confirms that the Au@Ag core-shell NC is a single-crystalline structure formed through the epitaxial growth of silver atoms on the gold ellipsoidal core. Besides, based on the above crystallographic analysis, a three dimensional (3D) model of the Au@Ag core-shell NC is reconstructed in Fig. 3(d) and shows that the ellipsoidal gold core is surrounded by a silver shell with the truncated cube morphology. This visual model will be used for the discussions of the growth mechanism of Au@Ag core-shell NCs and the simulations of optical-electric characteristics later.

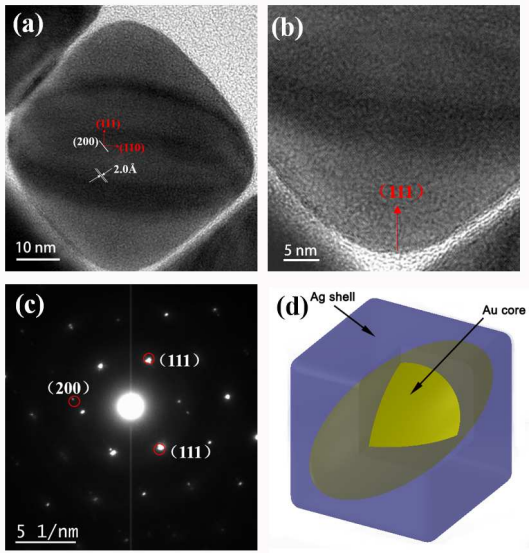

Fig. 3 High-resolution TEM images of (a) Au@Ag core-shell NC and (b) the truncated corner of nanocube, (c) SAED patterns and (d) 3D model of the Au@Ag core-shell NC. The One-eighth silver shell is uncovered to expose gold core in the Au@Ag core-shell NC, in (d).

3.3. Growth Mechanisms of the Au@Ag Core-shell NCs

Throughout the growth procedure of the heterogeneous binary-metal core-shell structures, many factors related with materials and growth kinetics are found to be crucial for the final shapes of the resultant nanocrystals, especially, surfactants and the surface energies of crystal.[6] In our experiments, three kinds of surfactants CTAB, CPC and CTAC were used to prepare the Au@Ag core-shell NCs. To elucidate the effects of the surfactants on the synthesis of nanoparticles, Fig. 4 gives the schematic illustration of the growth mechanism of Au@ Ag core-shell NCs starting from Au seeds to bimetallic cube.

In the synthesis step of Au NRs, short gold nanorods were prepared by the use of CTAB-stabilized gold seeds in the presence of silver ions.[37] During that time, CTAB molecules adsorb on gold nanorods in the form of bilayers steric interaction, i.e., the trimethylammonium headgroup in a monolayer facing to gold surface and the other facing the solvent to maintain water solubility.[38, 39] For the face centered cubic (fcc) crystals Au and Ag, their surface energies of the low-index crystallographic facets are given in the order $\gamma\{111\}<\gamma\{100\}<\gamma\{110\}$.[40] The CTAB bilayers absorbed on gold surface induces direct stacking of gold atoms along the direction [100] on facet {100} at the ends and blocking the side crystal facets {110} and {111}.[41, 42] Consequently the CTAB-stabilized gold seeds maintain slow growth on {110} side facets and faster growth on {100} end facets to form nanorod.[35] During the next step of the preparation of the Au NEs, CTAB was replaced with the surfactant CPC. At this time, the chloride anionics of CPC adsorb onto the gold surface through electrostatic forces and create a negatively charged layer, then binding with the cetylpyridinium cations.[33] However, such absorption exhibits poor stability on {110} side facet because of the relatively large surface energy and stress compared to other facets, which allows directional growth along the {110} facets to form an ellipsoidal shape.[43]

Subsequently, in the final step the Au NEs was used as seeds to synthesize the Au@Ag core-shell NCs. According to the Frank-van der Merwe mode, as a typical example of the epitaxial growth of heterogeneous core-shell nanocrystals, Au@Ag system has a small lattice mismatch (0.17%), the electronegativity of Ag is lower than that of Au, and the bond energy of Ag-Ag is smaller than that of Au-Ag.[20,44] In our case, it was found that Ag atoms were epitaxial grown on the surface of Au NE core into a truncated cube by means of the surfactant CTAC and the halide KBr. Here, CTAC was used to replace CPC and forms bilayer around Au NE core, similar to the arrangement way of CTAB molecules on the surface of Au NRs. And KBr was introduced into the growth solutions for bromide ions instead of chloride ions since bromide ion has a higher affinity with silver than chloride ion does.[45, 46] During the layer by layer epitaxial growth of Ag atoms on the surface of Au NE, combining the effects of the cationic surfactants and the bromide counterions, the thickness of the Ag shell increases along [110] direction of the Au ellipsoidal core, and then the {100} facets of silver shell were stabilized for cubic shaped growth. Finally, the Au@Ag core-shell NC was formed from an Au ellipsoid to a bimetallic cube.

3.4 SERS performance of the Au@Ag core-shell NCs.

To investigate the SERS behaviour of our Au@Ag core-shell NCs, the wavelength-dependent electric field enhancement is firstly calculated using FEM and shown in Fig. S4, and the electric field distribution of this bimetallic structure is then numerically simulated to evaluate the enhanced Raman signals at incident wavelength of 785 nm. As shown in Fig. 5(a), the bimetallic cube has the geometric parameters of edge length 55 nm and truncated corner 5 nm, Au ellipsoidal core with major-axis 66 nm and minor-axis 38 nm, which precisely match the experimental particle geometry. The incident light is polarized along the major-axis of the ellipsoid propagates parallel to the body diagonal plane of cube. Simultaneously, the model of 55 nm size edge-truncated pure Ag cube is shown in Fig. 5(b) for comparison. And the electric field intensity distributions for two

Physical Chemistry Chemical Physics Accepted Manuscript

This journal is © The Royal Society of Chemistry [year]

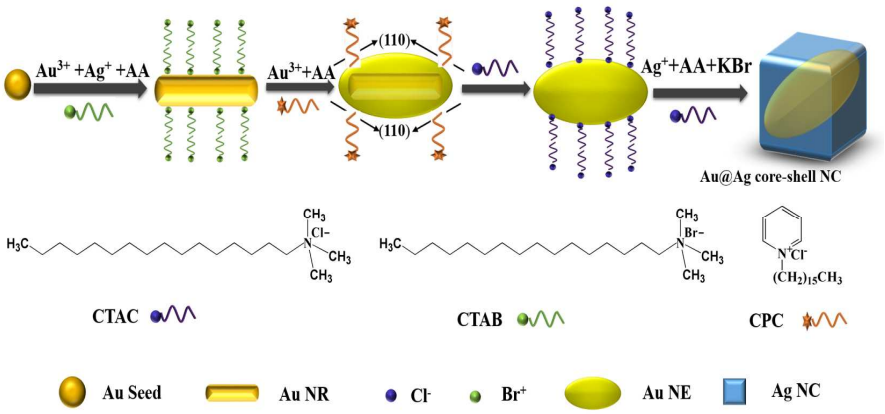

Fig. 4 Schematic of the growth mechanism of Au@ Ag core-shell NCs.

different types of nanocubes are shown in Fig. 5(a) and 5(b), respectively. The maximum electric field enhancement of the Au@Ag core-shell cube and the pure Ag cube are 27.4 and 18.1, respectively. It indicates that the electric-field enhancement of Au@Ag core-shell NC is much higher than of pure Ag NC.

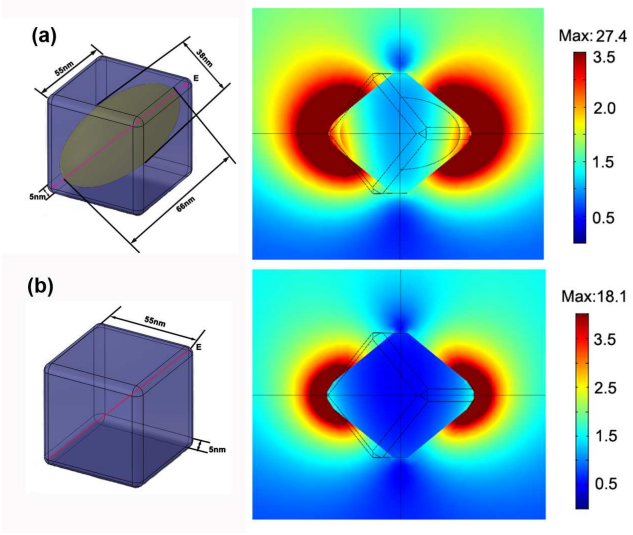

Fig. 5 The 3D models (left) and electric field distributions in tangent planes (right) of the Au@Ag core-shell NC (a) and the pure Ag NC (b), respectively.

It is interesting to explore the characteristic of the strong electromagnet enhancements of the Au@Ag core-shell NCs. For the cubic structure of ellipsoidal Au core encapsulated in the Ag shell, according to the plasmon hybridization theory, the weak shoulder around 550 nm in Fig. 2(c) origins from the hybridized plasmon resonances of the dipolar Ag cavity mode $|\omega_-\rangle$ and Au ellipsoid core modes ω_{core} (Fig. S5). And, the interaction strength of plasmonic modes of Ag cavity and Au ellipsoid core is controlled by the thickness of the Ag shell layer. In our case, the Ag shell thickness around the corner of the Au@Ag core-shell NCs is thinnest so that the plasmons modes of Au ellipsoid core are not completely screened and still discerned, which is similar to the case in ref. [47]. It is the plasmon hybridization of Au ellipsoid core and Ag shell which associated with electric field enhancement make the Au@Ag core-shell NCs amplify electrical signals.[48-49] As shown in Fig. 5(a), the maximum electric field enhancement occurs around two diagonal corners of the cube along the major axis of the Au ellipsoid, which means that, the plasmonic interactions are strongest in the intra-junctions of the thin Ag layers and the ends of Au ellipsoidal core. In contrast, weak plasmonic coupling occurs in other locations, especially the six corners of the cube except the two above-mentioned diagonal corners due to the thicker Ag layers. Obviously, the electric field distribution of the Au@Ag core-shell NCs depends critically on the local thickness of the Ag layer covering the Au ellipsoidal core. This is completely different from the case of pure Ag NC as shown in Fig. 5(b). The above analysis shows that the Au@Ag core-shell NCs generated much higher electric field intensity not only from the corner and edge of the cube but also from the plasmonic interaction of the core and the shell in the bimetallic nanostructure.

Next, the SERS performance of Au@Ag core-shell NCs is experimentally researched by 4-MBA as the Raman active molecules. For quantifying SERS enhancements of the Au@Ag NCs, the resonance enhancement and the chemical enhancement are minimized in our experiment because the 4-MBA is a non-resonant molecule under near-infrared excitation wavelength of 785 nm.[50] It allows us to particularly focus on only the electromagnetic contribution to the Raman enhancements.[51] Our previous work had shown that Ag NCs offer higher SERS signals than those of the Ag nanosphere.[52] Combining with the above theoretical analysis, it can be expected that the Au@Ag core-shell NCs should provide much higher electric field intensity due to plasmonic hybridization between the core and shell in the bimetallic nanostructure. Figure 6 gives the SERS spectra of the Raman active molecules 4-MBA linked with the as-prepared Au@Ag core-shell NCs. In Fig. 6, the SERS bands of 4-MBA display obvious fingerprint characteristics, for example, the two dominant Raman peaks at 1078 and 1590 cm^{-1} are ascribed to the ν(C-C) benzene ring-breathing modes, the peaks at 847 cm^{-1} and 1137 cm^{-1} originate from the COO- bending mode (δ(COO-)) and the mixed mode (13β(CCC)+ν(C-S)+ ν(C-COOH)), and a stretching mode at 1430 cm^{-1} (νs(COO-)).[53, 54] Due to the strong coupling between the transition dipole moment of benzene ring and local electric field, the ν(C-C) mode shows a prominent intensity than that of the other modes. Consequently, we used the intensity of the peak at 1078 cm^{-1} to evaluate the SERS performance of Au@Ag core-shell NCs.

Here, the enhancement factor (EF) is estimated by comparing the SERS signals from the 4-MBA labeled nanoparticle solutions to the Raman intensities obtained from pure 4-MBA solution. The calculation of enhancement factor follows the equation: $EF=(I_{SERS}/I_{normal})\times(N_{normal}/N_{SERS})$, where I_{SERS} and I_{normal} are the integrated intensities of the same band in the SERS and normal

Physical Chemistry Chemical Physics Accepted Manuscript

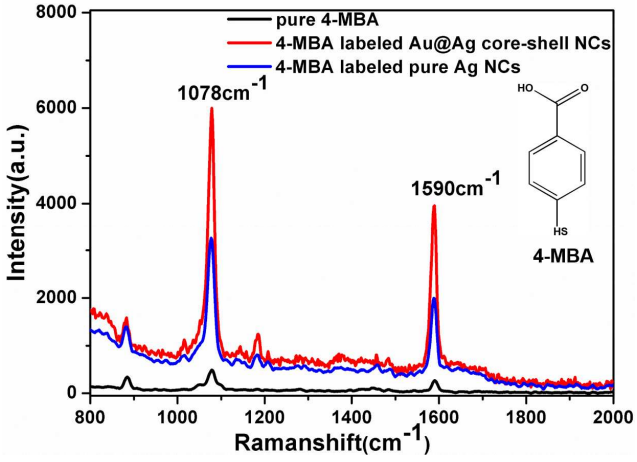

Fig. 6 Raman spectra of 4-MBA labeled Au@Ag core-shell NCs (red curve), 4-MBA labeled pure Ag NCs (blue curve) and pure 4-MBA (black curve)

Raman spectra under the same conditions, respectively; N_{normal} and N_{SERS} separately are the molecule number of the 4-MBA sample and the 4-MBA adsorbed on the nanoparticles, which are probed in the effective excitation volume of the laser.[50] To calculate the "normal" values of the EF, Raman signal of the 4-MBA sample solution (10 mM) was recorded by the Raman spectrometer. The diameter of the illumination focus 2.39 μm was first calculated using the following equation: $D_{diameter} = (\lambda/NA) \times 1.22$, in which the NA of the 20 × objective lens of the Raman spectrometer was 0.4 and the wavelength of the excitation laser was 785 nm; [54] besides, the penetration depth of 785 nm laser beam is about 6.53 μm in the solution. [55, 56] Then, the effective excitation volume was 60.65 μm^3, and the $N_{normal} = 3.63\times10^8$. Next, under the same measurement conditions, $N_{SERS} = 1.47\times10^3$ was obtained for the 1mL solution of 4-MBA-labeled Au@Ag core-shell NCs in a 2 mm quartz cuvette. And from Fig. 6, the experimental values of $I_{normal\ (4\text{-}MBA)}$, $I_{SERS\ (Au@Ag)}$ and $I_{SERS\ (pure\ Ag)}$ are 1.52×10^4, 9.62×10^4 and 1.61×10^5, respectively. Thus, the EF value of the Au@Ag core-shell NCs is calculated as $EF_1 = 2.27\times10^6$ and for pure Ag NCs, $EF_2 = 1.43\times10^6$. Thus such Au@Ag core-shell NCs exhibit higher SERS efficiency than that of Ag NCs and well stability (Fig. S6). It is in very good agreement with the calculation results shown in Fig. 5, that is, the core-shell nanostructure engenders stronger electric field intensity leading to higher SERS enhancement. Those provide evidence to support that Au@Ag core-shell NCs exhibit superior SERS property and can be an excellent candidate for SERS-based analysis.

4. Conclusions

In summary, the Au@Ag core-shell NCs have been fabricated by an epitaxial growth method. The geometry of the bimetal core-shell structure can be deliberately controlled through the growth kinetic process from Au NEs to hetero-structure cube, with using the different type of surfactants. It also allows us to control the LSPR characteristic and the SERS capability of the Au@Ag core-shell NCs. The theoretical analysis demonstrates that Au@Ag core-shell NCs involving the strongly plasmonic coupling of confined in nanoscale intra-junctions of Au core and Ag shell may provide sufficiently high electric field enhancements. And the experimental results show that the Au@Ag core-shell NCs exhibit stronger SERS enhancements with an EF of 10^6 at 785 nm excitation, which is comparable with that of pure Ag NCs. Therefore, the above research may guide the design and fabrication of bimetallic nanoparticles with increasing geometric complexity and further optimized plasmonic properties, and then further implement sufficiently enhanced Raman signals for potential application in biosensing and bioimaging.

Acknowledgement

This work was supported by the National Natural Science Foundation of China (Grant Nos. 61275153, 61320106014 and 11404177); the Natural Science Foundation of Zhejiang (Grant No. LY12A04002); the Natural Science Foundation of Ningbo (Grant Nos. 2012A610107 and 2014A610120), and K. C. Wong Magna Foundation of Ningbo University, China. CUHK1/CRF/1G Collaboration Research Fund from the Hong Kong Research Grants Council.

Notes and references

[a] *Institute of Photonics, Faculty of Science, Ningbo University, Ningbo 31†5211, Zhejiang, China. Tel: +86-574-87600794; Fax: +86-574-87600744; E-mail: zhoujun@nbu.edu.cn*
[b] *Department of Electronic Engineering, The Chinese University of Hong Kong, Hong Kong Special Administrative Region, China.*
[c] *Institute of Cybernetics "E. Caianiello" of CNR, Via Campi Flegrei 34, 80072 Pozzuoli, Italy*

1 C. J. Murphy, T. K. Sau, A. M. Gole, C. J. Orendorff, J. Gao, L. Gou, S. E. Hunyadi and T. Li, J. Phys. Chem. B, 2005, **109**, 13857-13870.
2 Z. L. Wang, J. Phys. Chem. B, 2000, **104**, 1153-1175.
3 E. Hao, G. Schatz and J. Hupp, J. Fluoresc, 2004, **14**, 331-341.
4 R. W. J. Scott, O. M. Wilson and R. M. Crooks, J. Phys. Chem. B, 2004, **109**, 692-704.
5 C. J. Murphy, A. M. Gole, S. E. Hunyadi and C. J. Orendorff, Inorg. Chem., 2006, **45**, 7544-7554.
6 Y. Xia, X. Xia, Y. Wang and S. Xie, Mater. Res. Bull., 2013, **38**, 335-344.
7 S. Eustis and M. A. El-Sayed, Chem. Soc. Rev., 2006, **35**, 209-217.
8 M. Rycenga, C. M. Cobley, J. Zeng, W. Li, C. H. Moran, Q. Zhang, D. Qin and Y. Xia, Chem. Rev., 2011, **111,** 3669-3712.
9 Y. Xia, P. Yang, Y. Sun, Y. Wu, B. Mayers, B. Gates, Y. Yin, F. Kim and H. Yan, Adv. Mater., 2003, **15**, 353-389.
10 L. Zhang, W. Niu and G. Xu, Nano Today, 2012, **7**, 586-605.
11 Y. Huang, L. Hu, T. Zhang, H. Zhong, J Zhou, Z. Liu, H. Wang, Z. Guo and Q. Chen, Sci. Rep., 2013, **3**, 2647.
12 M. Sun and H. Xu, Small, 2012, 8, 2777-2786.
13 K. Park, L. F. Drummy and R. A. Vaia, J. Mater. Chem., 2011, **21**, 15608-15618.
14 C. J. DeSantis, R. G. Weiner, A. Radmilovic, M. M. Bower and S. E. Skrabalak, J. Phys. Chem. Lett., 2013, **4**, 3072-3082.
15 X. Teng, W. Han, Q. Wang, L. Li, A. I. Frenkel and J. C. Yang, J. Phys. Chem. C, 2008, **112**, 14696-14701.
16 Y. Lu, J. Yuan, F. Polzer, M. Drechsler and J. Preussner, ACS Nano, 2010, **4**, 7078-7086.
17 M. Sharma, P. R. Pudasaini, F. Ruiz-Zepeda, E. Vinogradova and A. A. Ayon, ACS Appl. Mater. Inter., 2014, **6**, 15472-15479.
18 M. Tsuji, R. Matsuo, P. Jiang, N. Miyamae, D. Ueyama, M. Nishio, S. Hikino, H. Kumagae, K. S. N. Kamarudin and X.-L. Tang, Crys. Growth Des., 2008, **8**, 2528-2536.
19 Nie and S. R. Emory, Science, 1997, **275**, 1102-1106.
20 E. C. Cho, P. H. C. Camargo and Y. Xia, Adv. Mater., 2010, **22**, 744-748.

Physical Chemistry Chemical Physics Accepted Manuscript

This journal is © The Royal Society of Chemistry [year]

21 F.-R. Fan, D.-Y. Liu, Y.-F. Wu, S. Duan, Z.-X. Xie, Z.-Y. Jiang and Z.-Q. Tian, J. Am. Chem. Soc., 2008, **130**, 6949-6951.

22 Y. Xiang, X. Wu, D. Liu, Z. Li, W. Chu, L. Feng, K. Zhang, W. Zhou and S. Xie, Langmuir, 2008, **24**, 3465-3470.

23 J. H. Song, F. Kim, D. Kim and P. Yang, Chem.-Eur. J., 2005, **11**, 910-916.

24 L. Cui, A. Wang, D.-Y. Wu, B. Ren and Z.-Q. Tian, J. Phys. Chem. C, 2008, **112**, 17618-17624.

25 Y. Ma, W. Li, E. C. Cho, Z. Li, T. Yu, J. Zeng, Z. Xie and Y. Xia, ACS Nano, 2010, **4**, 6725-6734.

26 26 J. Gong, F. Zhou, Z. Li and Z. Tang, Langmuir, 2012, 28, 8959-8964.

27 M. Fernanda Cardinal, B. Rodríguez-González, R. n. A. Alvarez-Puebla, J. Pérez-Juste and L. M. Liz-Marzán, J. Phys. Chem. C, 2010, **114**, 10417-10423.

28 G. Park, C. Lee, D. Seo and H. Song, Langmuir, 2012, **28**, 9003-9009.

29 J. Gong, F. Zhou, Z. Li and Z. Tang, Chem. Commun., 2013, **49**, 4379-4381.

30 A. K. Samal, L. Polavarapu, S. Rodal-Cedeira, L. M. Liz-Marzán, J. Pérez-Juste and I. Pastoriza-Santos, Langmuir, 2013, **29**, 15076-15082.

31 H. Jing, N. Large, Q. Zhang and H. Wang, J. Phys. Chem. C, 2014, **118**, 19948-19963.

32 B. Nikoobakht and M. A. El-Sayed, Chem. Mater., 2003, **15**, 1957-1962.

33 W. Niu, S. Zheng, D. Wang, X. Liu, H. Li, S. Han, J. Chen, Z. Tang and G. Xu, J. Am. Chem. Soc., 2008, **131**, 697-703.

34 P. B. Johnson and R. W. Christy, Phys. Rev. B, 1972, **6**, 4370-4379.

35 C. J. Murphy, L. B. Thompson, A. M. Alkilany, P. N. Sisco, S. P. Boulos, S. T. Sivapalan, J. A. Yang, D. J. Chernak and J. Huang, J. Phys. Chem. Lett., 2010, **1**, 2867-2875.

36 E. Ringe, J. M. McMahon, K. Sohn, C. Cobley, Y. Xia, J. Huang, G. C. Schatz, L. D. Marks and R. P. Van Duyne, J. Phys. Chem. C, 2010, **114**, 12511-12516..

37 S. Lee, L. J. E. Anderson, C. M. Payne and J. H. Hafner, Langmuir, 2011, **27**, 14748-14756.

38 B. Nikoobakht and M. A. El-Sayed, Langmuir, 2001, **17**, 6368-6374.

39 D. K. Smith and B. A. Korgel, Langmuir, 2008, **24**, 644-649.

40 40 F. Tian, F. Bonnier, A. Casey, A. E. Shanahan and H. J. Byrne, Anal. Methods, 2014.

41 T. K. Sau and C. J. Murphy, Langmuir, 2005, **21**, 2923-2929.

42 T. H. Ha, H.-J. Koo and B. H. Chung, J. Phys. Chem. C, 2006, **111**, 1123-1130.

43 A. M. Alkilany and C. J. Murphy, Langmuir, 2009, **25**, 13874-13879.

44 A. K. Samal, L. Polavarapu, S. Rodal-Cedeira, L. M. Liz-Marzán, J. Pérez-Juste and I. Pastoriza-Santos, Langmuir, 2013, **29**, 15076-15082.

45 S. E. Lohse, N. D. Burrows, L. Scarabelli, L. M. Liz-Marzán and C. J. Murphy, Chem. Mater., 2013, **26**, 34-43.

46 S. Gómez-Graña, B. Goris, T. Altantzis, C. Fernández-López, E. Carbó-Argibay, A. Guerrero-Martínez, N. Almora-Barrios, N. López, I. Pastoriza-Santos, J. Pérez-Juste, S. Bals, G. Van Tendeloo and L. M. Liz-Marzán, J. Phys. Chem. Lett., 2013, **4**, 2209-2216.

47 Y. Chen, H. Wu, Z. Li, P. Wang, L. Yang and Y. Fang, Plasmonics, 2012, **7**, 509-513.

48 N. J. Halas, S. Lal, W.-S. Chang, S. Link and P. Nordlander, Chem. Rev., 2011, **111**, 3913-3961.

49 D.M. Mott, D.T. Anh, P. Singh, C. Shankar and S. Maenosono, Adv. Colloid Interface Sci., 2012, **185-186**, 14-33.

50 R. A. Álvarez-Puebla, J. Phys. Chem. Lett., 2012, **3**, 857-866.

51 Q. Zhang, N. Large and H. Wang, ACS Appl. Mater. Inter., 2014, **6**, 17255-17267

52 T. Jiang, L. Zhang and J. Zhou, Analyst, 2014, **139**, 5894-5901.

53 A. Michota and J. Bukowska, J. Raman Spectrosc., 2003, **34**, 21-25.

54 Y. He, S. Su, T. T. Xu, Y. L. Zhong, J. A. Zapien, J. Li, C. H. Fan, S. T. Lee, Nano Today, 2011, **6**, 122–130.

55 A. Michota, J. Bukowska, J. Raman Spectrosc., 2003, **34**, 21-25.

56 V.S. Tiwari, T. Oleg, G.K. Darbha, W. Hardy, J.P. Singh and P.C. Ray, J. Phys. Chem. Lett.,2007, 446, 77-82.

Physical Chemistry Chemical Physics Accepted Manuscript